Cr fluorescence spectrum. Thus, we would expect that a breakdown of Cr-doped $MgSiO_3$ to its oxide components would also result in such a fluorescence spectrum (*25*). The lack of phase transitions in MgO additionally allowed measurements with higher sensitivity on the recovered samples outside the diamond cell. We found no MgO after heating $MgSiO_3$ glass, doped with 0.1 atomic % Cr^{3+}, in an argon medium at 3000 K and 73 GPa for 10 min (Fig. 4, A and B). Instead, the recovered perovskite crystal (Fig. 4C) exhibits two prominent fluorescence peaks at 710.2 and 714 nm (Fig. 4B).

We have shown that silicate perovskite heated with small temperature gradients in a quasi-hydrostatic pressure medium does not decompose to its component oxides and that instead these oxides react to form perovskite when heated to the highest pressures in our experiments (100 GPa). These results are important in view of new evidence for a dense high-pressure polymorph of SiO_2 (*26*), because they show that, at the present pressure and temperature conditions, (Mg,Fe)SiO_3-perovskite is more dense than a (Mg,Fe)O-SiO_2 assemblage.

REFERENCES AND NOTES

1. E. Knittle and R. Jeanloz, *Science* **235**, 668 (1987).
2. N. Funamori and T. Yagi, *Geophys. Res. Lett.* **20**, 387 (1993).
3. C. Meade, H. K. Mao, J. Hu, *Science* **268**, 1743 (1995).
4. S. K. Saxena *et al.*, *ibid.* **274**, 1357 (1996).
5. We laser-heated samples in a large variety of pressure media and found that the laser power required in a NaCl pressure medium is markedly higher than that for CsCl or KBr media. This result is consistent with a comparative study of several alkali halides, where the thermal conductivity of NaCl in the B2 structure was estimated to be at least three times that of CsCl [G. A. Slack and R. G. Ross, *J. Phys. C* **18**, 3957 (1985)].
6. We measured temperature fluctuations in silicate samples using unstabilized CO_2 laser techniques of order 1000 K.
7. YAG laser heating without thermally insulating media causes temperature gradients in silicates ranging from 100° to 1000° per micrometer depending on the peak temperature [D. L. Heinz and R. Jeanloz, *J. Geophys. Res.* **92**, 11437 (1987)].
8. A. J. Campbell and D. Heinz, *Geophys. Res. Lett.* **19**, 1061 (1992).
9. H.-k. Mao, G. Shen, R. J. Hemley, *Science* **278**, 2098 (1997).
10. Y. Fei, Y. Wang, L. W. Finger, *J. Geophys. Res.* **101**, 11525 (1996).
11. R. Boehler and A. Chopelas, in *High Pressure Research: Applications to Earth and Planetary Sciences*, Y. Syono and M. H. Manghnani, Eds. (American Geophysical Union, Washington, DC, 1992), pp. 55–60.
12. A. Chopelas and R. Boehler, in *High Pressure Research: Applications to Earth and Planetary Sciences*, Y. Syono and M. H. Manghnani, Eds. (American Geophysical Union, Washington, DC, 1992), pp. 101–108.
13. R. Boehler and A. Zerr, *Science* **264**, 280 (1994).
14. The emitted light from the sample was measured from areas of 2 to 3 μm in diameter in the center of the hot spot with a charge-coupled device (CCD) detector in the wavelength range of 500 to 815 nm. Emissivity was taken to be independent of the wavelength.
15. We used MgO and SiO_2 with 99.999% purity. $Mg_{0.85}Fe_{0.15}O$ was provided by S. Kesson (Australian National University). Powder mixtures with 1- to 2-μm grain size were compressed at about 5 GPa with a DAC to form pellets with about 10-μm thickness.
16. The orthoenstatite sample was from the Smithsonian Institute (#137311).
17. Cr-doped $MgSiO_3$ glass samples were provided by S. Kesson and were also synthesized from stoichiometric amounts of MgO and SiO_2 quartz powders of 99.999% purity and Cr_2O_3 of 99.5% purity by melting with a CO_2 laser and rapid quenching between two platinum-plated copper blocks.
18. A. Chopelas, *Phys. Earth Planet. Inter.* **98**, 3 (1996).
19. J. K. Kingma, R. E. Cohen, R. J. Hemley, H. K. Mao, *Nature* **374**, 243 (1995).
20. The linear extrapolation of the Raman frequencies from 65 GPa (*18*) agrees with those found here to 100 GPa, except for the highest wavenumber mode, which at the highest pressure is 13 cm^{-1} lower. Upon pressure release, the position of the Raman modes matches those measured previously.
21. The strongest Raman mode in the post-stishovite phase (*19*) would appear at 950 cm^{-1} at 70 GPa. To check whether some other phase of SiO_2 had formed, we released the pressure in our experiments to within the stability field of stishovite, because the reported high-pressure polymorphs of SiO_2 were found to revert to the stishovite phase upon pressure release (*19*, *26*). We did not detect any Raman mode of stishovite, the strongest of which would appear, for example, at 801 cm^{-1} in the spectrum taken at 15 GPa (Fig. 3B).
22. G. Serghiou, A. Zerr, A. Chopelas, R. Boehler, *Phys. Chem. Miner.* **25**, 193 (1998).
23. A. Chopelas, in *Mineral Spectroscopy: A Tribute to Roger Burns*, M. D. Dyar, C. McCammon, M. W. Schaefer, Eds. (Special Publication 5, Geochemical Society, Columbus, OH, 1996), pp. 229–242.
24. Raman and fluorescence spectra from the samples were excited with the 457.9-nm line of a Spectra Physics 2025-5 argon ion laser. The laser light entered the diamond cell at an incident angle of 25° and was focused to a 15-μm spot on the sample with powers ranging from 5 to 100 mW depending on pressure. The signal was detected with a liquid nitrogen–cooled CCD detector or a photomultiplier. Spectra were taken at room temperature from the laser-heated spot.
25. Cr^{3+} on part per million levels in MgO crystals has been detected by this method [A. M. Glass, *J. Chem. Phys.* **46**, 2080 (1967)].
26. L. S. Dubrovinsky *et al.*, *Nature* **388**, 362 (1997).

27. We thank A. Chopelas, O. Tschauner, V. Hillgren, and L. Nigay for many helpful discussions.

10 March 1998; accepted 12 May 1998

Perennial Antarctic Lake Ice: An Oasis for Life in a Polar Desert

John C. Priscu,* Christian H. Fritsen, Edward E. Adams, Stephen J. Giovannoni, Hans W. Paerl, Christopher P. McKay, Peter T. Doran, Douglas A. Gordon, Brian D. Lanoil, James L. Pinckney

The permanent ice covers of Antarctic lakes in the McMurdo Dry Valleys develop liquid water inclusions in response to solar heating of internal aeolian-derived sediments. The ice sediment particles serve as nutrient (inorganic and organic)–enriched microzones for the establishment of a physiologically and ecologically complex microbial consortium capable of contemporaneous photosynthesis, nitrogen fixation, and decomposition. The consortium is capable of physically and chemically establishing and modifying a relatively nutrient- and organic matter–enriched microbial "oasis" embedded in the lake ice cover.

The McMurdo Dry Valleys, Antarctica, is one of the coldest and driest deserts on Earth. Lakes in this region are permanently ice covered (*1*). The ice is typically 3 to 6 m thick and contains a layer of sand and organic matter of aeolian origin below the surface. This layer represents a dynamic equilibrium between downward movement of sediments as a result of melting during the summer and upward movement of ice from ablation at the surface and freezing at the bottom. Liquid water inclusions are present in this layer for about 150 days during the summer when solar radiation is continuous; up to 40% of the total ice cover volume during this period can be liquid water (*2*, *3*). We discovered that the ice meltwater supports a viable microbial assemblage associated with the sediment layer. Here, we describe the ecosystem.

We collected ice samples from six lakes (Bonney, Hoare, Fryxell, Miers, Vanda, and Vida) between August and October 1993 and 1995 using 10-cm-diameter coring devices. Cores were sectioned, melted, and analyzed for photoautotrophic and heterotrophic activity; biomass, sediment, and nitrous oxide content; and chemistry (*4*). Most of

J. C. Priscu and C. H. Fritsen, Department of Biological Sciences, Montana State University, Bozeman, MT 59717, USA.
E. E. Adams, Department of Civil Engineering, Montana State University, Bozeman, MT 59717, USA.
S. J. Giovannoni, D. A. Gordon, B. D. Lanoil, Department of Microbiology, Oregon State University, Corvallis, OR 97331, USA.
H. W. Paerl and J. L. Pinckney, Institute of Marine Sciences, University of North Carolina at Chapel Hill, Morehead City, NC 28557, USA.
C. P. McKay, Space Science Division, NASA Ames Research Center, Moffet Field, CA 94035, USA.
P. T. Doran, Earth and Environmental Sciences, University of Illinois at Chicago, Chicago, IL 60607, USA.
*To whom correspondence should be addressed.

our studies were on Lake Bonney. The ice cover of Lake Bonney was 4 m thick, and the sediment layer was 2 m beneath the ice surface (Fig. 1A). N_2O and dissolved inorganic nitrogen (DIN) (NH_4^+ + NO_2^- + NO_3^- = DIN) reached a maximum at this depth, indicating that the region was a source for nitrogen (Fig. 1, A and B). N_2O is a known intermediate of nitrification in the liquid water column of this lake (*5*). Soluble reactive phosphorus (SRP) showed no clear trend with depth. The DIN:SRP ratio averaged 31.3 (range of 20.3 to 107.7), indicative of phosphorus deficiency (*6*). N_2 fixation (*7*) ranged from 9.4 to 91.3 nmol of N_2 per milligram of chlorophyll *a* per hour in lake ice aggregates. Primary productivity, bacterial activity, chlorophyll *a* concentration, and bacterial cell number also were highest in or near this sediment layer (*8*) (Fig. 1, C and D). Dissolved organic carbon (DOC) was highest near the peaks in primary and bacterial productivity. Primary productivity ranged up to 7.8 μg of C per liter per day, and bacterial productivity ranged up to 0.40 nM thymidine per day in the combined data set from all six lakes. High photoautotrophic biomass was associated with high bacterial biomass in the combined data set.

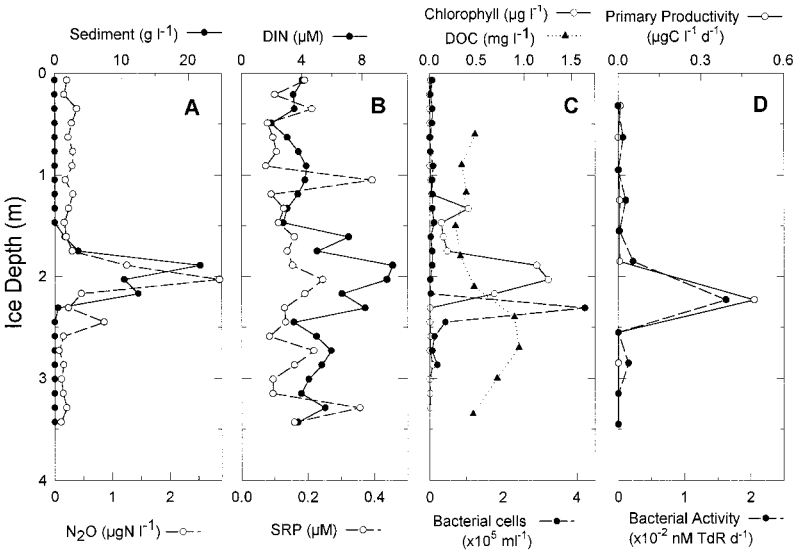

Fig. 1. (**A** to **D**) Vertical profiles of selected constituents in the lake ice cover of Lake Bonney (*8*). TdR, incorporation of ^{3}H-thymidine.

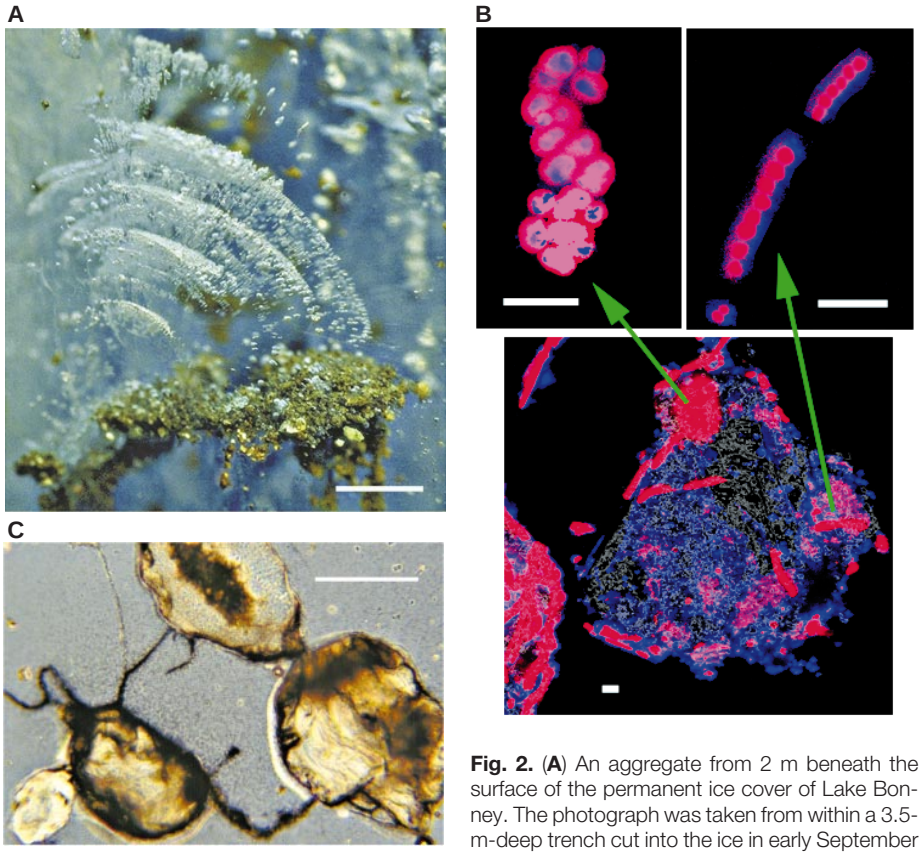

Fig. 2. (**A**) An aggregate from 2 m beneath the surface of the permanent ice cover of Lake Bonney. The photograph was taken from within a 3.5-m-deep trench cut into the ice in early September before the formation of liquid water. Scale bar, 2 cm. (**B**) Confocal laser photomicrographs showing microorganisms associated with a sediment particle, with enlarged views of two species of cyanobacteria (blue, DAPI-stained bacteria; red, chlorophyll autofluorescence; gray, sediment particle). Scale bars, 10 μm. (**C**) Microautoradiograph of sediment particles bound by cyanobacterial filaments (dark regions denote sites of active $^{14}CO_2$ accumulation, indicative of photosynthetic activity). Scale bar, 100 μm.

A complex microbial assemblage was physically associated with the sediment. The sediment is composed of aggregated sand and gravel, distributed in centimeter-scale inclusions within the ice when no liquid water is present (Fig. 2A). Bubbles present above the sediment layer likely formed from gas exsolution as the liquid water lens froze from the top downward during early winter (*2*, *3*). Confocal microscopy (*9*) revealed bacterial and cyanobacterial cells attached to the sediment particles (Fig. 2B). Most of the cyanobacteria are filamentous species of the genus *Phormidium* (Fig. 2B, top right). More rarely, we observed cells of the cyanobacterial genus *Chamaesiphon* (Fig. 2B, top left), the nitrogen-fixing genus *Nostoc*, unidentified coccoidal cyanobacteria, and diatom algae. Phylogenetic analysis (*10*) of the oxygenic phototrophs was performed by cloning bacterial 16S ribosomal RNA genes directly from the ice assemblage DNA (Fig. 3). Thirty-one of the 198 bacterial genes sequenced were of cyanobacterial origin; among these were four clades. Three clades were allied with the genera *Leptolyngbya*, *Chamaesiphon*, and *Phormidium*. The fourth could not be associated with any of the cyanobacterial genes in public sequence databases. These observations establish that representatives of widely distributed cyanobacterial groups have successfully colonized the ice habitat. The lake ice organisms do not resemble the predominantly eukaryotic plankton within the water column of Lake Bonney.

Our data imply that ice sediment particles serve as nutrient (inorganic and organic)-enriched microzones for the establishment of a physiologically and ecologically complex microbial consortium capable of contemporaneous photosynthesis, N_2 fixation, and decomposition. All of

these processes are needed to complete essential nutrient cycles. CO_2- and N_2-fixing capabilities ensure access to biologically available carbon and nitrogen, key growth-limiting nutrients in aquatic and terrestrial habitats. Microautoradiography revealed that filamentous cyanobacteria actively fix CO_2 upon exposure to meltwater (Fig. 2C). Microautoradiographs also show that bacteria are capable of metabolizing a range of organic substrates closely associated with cyanobacteria (*11*). These activities imply a consortial arrangement within the assemblage where photoautotrophs are supplying fixed carbon (and nitrogen in the case of N_2-fixing species) and heterotrophs are cycling CO_2 and inorganic nutrients back to the photoautotrophs. Highest dissolved inorganic carbon (DIC) concentration (1.2 mg of C liter^{-1}) corresponded to the region of greatest metabolic activity. Substrate kinetics experiments showed that DIC in this region does not limit photosynthetic activity. Microscopy also revealed that cyanobacterial filaments bind sediment particles, forming a cohesive fabric that produces a relatively nonfriable aggregate (Fig. 2C). Our data support the contention that this assemblage is capable of physically and chemically establishing and modifying a relatively nutrient- and organic matter–enriched microbial "oasis" embedded in the lake ice cover.

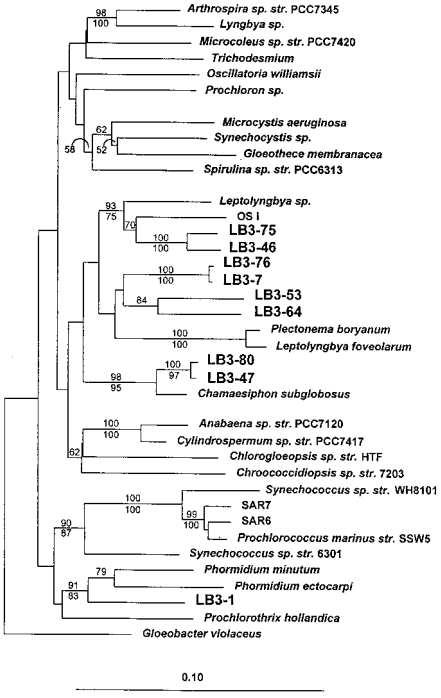

Fig. 3. Phylogenetic tree illustrating relations among selected 16S ribosomal DNA clones from the ice cover on Lake Bonney (clones from this study are designated LB3) and representative cyanobacterial sequences. The number of bootstrap replicates that supported each branch, from a total of 100 replicates, is shown above (neighbor-joining) and below (parsimony) each node. Bootstrap values below 50% are not shown. The 16S ribosomal DNA sequence of *Escherichia coli* was used to root the tree.

A model of sediment and associated particulate organic carbon (POC) dynamics within the ice cover of Lake Bonney illustrates the dominant physical and biological processes relevant to the transport and production of POC in this system. Aeolian transport is the primary allochthonous source of sediment and POC to the lake ice. The sediments and associated POC migrate to the depth in the ice in dynamic equilibrium with radiation-induced downward melting caused by sensible heating and with the net upward movement of the ice (*3*, *12*). Data from thermocouples embedded in the ice and observations from ice-core data indicate that meltwater in association with the sedimentary layers is present from November to February (*3*) and supports photosynthetic carbon production during this period of continuous sunlight (*13*, *14*). Daily average photosynthetically available radiation (PAR) reaching the photosynthetic layer ranged from 50 to 200 μmol of photons m^{-2} s^{-1} during the period of liquid water (*14*). We estimated that the median growth rate of photoautotrophs is 0.5 year^{-1} (range = 0.08 to 1.6 year^{-1}) using rates of photoautotrophic protein synthesis (*14*).

POC is lost from the ice cover through cracks and meltwater conduits that develop during the austral summers. We evaluated the POC balance within the ice cover of Lake Bonney using the following numerical relation in concert with data collected on the system:

$$\frac{\partial C}{\partial t} = (\mu \cdot C_i) + Q_a - Q_w$$

where C is the POC concentration per area, *t* is time, μ is the photoautotrophic growth rate (0.5 year^{-1}), C_i is the standing stock of microalgal POC in the ice (375 mg of C m^{-2}) (*15*), Q_a is the aeolian flux of POC onto the lake ice (43 mg of C m^{-2} year^{-1}) (*15*), and Q_w is the sinking flux of POC from the ice (2.3 mg of C m^{-2} year^{-1}) (*15*). This model represents net fluxes of POC only, neglecting losses to DOC and CO_2.

Our data imply that 229 mg of POC m^{-2} year^{-1} accumulated in the Lake Bonney ice cover during our study. The model predicts an unsteady-state condition where both POC and sediment accumulate over the year. These dynamics are expected to vary annually as local climate conditions affect PAR, aeolian deposition, and sediment loss from the ice cover. The model indicates that >80% of the computed POC accumulation results from carbon produced by cyanobacterial photosynthesis despite low growth rates and shows that the permanent ice covers provide viable habitats for the microscale proliferation of life in what would appear to be an otherwise inhospitable macroscale environment. The physical and biological dynamics of the permanent ice covers we describe differ from that in marine pack ice (*16*) and winter ice of temperate lakes (*17*). Both of these systems are characterized by freeze-flood cycles driven by snow deposition and are inhabited by organisms originating from the underlying liquid water column. Conversely, the microbial habitats in the ice covers of the dry valley lakes arise from internal melting associated with aeolian-deposited sediments, which also provides the biological seed.

The habitat in the Antarctic lake ice may serve as a model for life on Mars and Europa. Although Mars may have had extensive liquid water at one time, it rapidly cooled, and ice would have become, as it is today, the dominant form of water on the surface (*18*, *19*). On Europa, surface ice appears to exist in contact with subsurface liquid water (*20*–*22*). Solar heating of the subsurface could result in melt layers similar to those we describe here.

REFERENCES AND NOTES

1. C. P. McKay, G. D. Clow, R. A. Wharton, S. W. Squyres, *Nature* **313**, 561 (1985).
2. E. E. Adams, J. C. Priscu, C. H. Fritsen, S. R Smith, S. L. Brackman, in *Antarctic Research Series*, vol. 72, J. Priscu, Ed. (American Geophysical Union, Washington, DC, 1998), pp. 281–296.
3. C. H. Fritsen, E. A. Adams, C. P. McKay, J. C. Priscu, in *ibid*., pp. 269–280.
4. Cores were sectioned at 14- or 30-cm intervals, placed in bottles, and melted at 1° to 2°C. Cores for N_2O analysis were melted in gas-tight bottles; N_2O in the headspace gas was determined by gas chromatography (*5*). Subsamples of ice-core meltwater were filtered through Whatman GF/F filters that were extracted in cold dimethylsulfoxide:acetone:H_2O solution (50:45:5 by volume) for 12 to 24 hours. Chlorophyll *a* in the extracts was determined fluorometrically. Filtrate from the chlorophyll samples was analyzed for DIN and SRP [T. R. Parsons, Y. Maita, C. M. Lalli, *Manual of Chemical and Biological Methods for Seawater Analysis* (Pergamon, New York, 1984)] and DOC (Ocean Instruments 700 carbon analyzer). Samples for bacterial enumeration were stained with acridine orange and counted by epifluorescent microscopy [J. E. Hobbie, R. J. Daley, S. Jasper, *Appl. Environ. Microbiol*. **33**, 1225 (1977)]. Remaining sediments were then dried (90°C for 24 hours) and weighed. Subsamples were removed from core meltwater and incubated with either ^{14}C-labeled bicarbonate (8 μCi ml^{-1}) or ^{3}H-labeled thymidine (0.4 μCi ml^{-1}) for photoautotrophic and bacterial activity measurement, respectively. Samples for photosynthetic activity were incubated for 20 hours at 1°C and 100 μmol of photons m^{-2} s^{-1} before filtration through Whatman GF/F filters. The activity on the filters, together with DIC concentration, obtained from infrared analysis of gas-sparged samples, was used to compute photosynthetic rates. Samples for bacterial activity were incubated with 20 nM thymidine for 20 hours at 1°C in the dark followed by the addition of cold trichloroacetic acid (5% final concentration); samples were filtered on 0.2-μm filters for determination of isotopic incorporation.
5. J. C. Priscu, *Global Change Biol*. **3**, 301 (1997).

6. A. C. Redfield, *Am. Sci*. **46**, 205 (1958).
7. N_2 fixation was estimated by acetylene reduction [R. J. Flett, R. D. Hamilton, N. E. R. Campbell, *Can. J. Microbiol*. **22**, 43 (1976)] on liquid samples melted slowly. Incubations were at 1°C and 100 μmol of photons m^{-2} s^{-1} for 20 to 36 hours. A conversion factor of 0.33 (moles of N_2 fixed per mole of C_2H_2 produced) was used to estimate N_2 fixation rates from ethylene production.
8. The vertical offset between microbial biomass and activity maxima in Fig. 1, C and D, reflects variation between core samples and core length used for the analyses (14-cm core sections were used for data in Fig. 1, A to C; 30-cm sections were used for data in Fig. 1D). Because sediment aggregates occurred in relatively compact layers, rates would be higher if measured on shorter core sections incorporating the sediment layer only.
9. Lyophilized sediments for confocal microscopy were stained with 4′,6′-diamidino-2-phenylindole (DAPI) (1 mg ml^{-1}) and examined on a Leica laser scanning confocal microscope. Microautoradiography [H. W. Paerl and E. A. Stull, *Limnol. Oceanogr*. **24**, 1166 (1979)] was performed on slowly melted ice-core samples incubated at 4°C for 8 hours with ^{14}C-labeled bicarbonate (0.5 μCi ml^{-1}) at 100 μmol of photons m^{-2} s^{-1}.
10. DNA was extracted from sediments in the lake ice with guanidinium isothiocyanate [D. G. Pitcher, N. A. Saunders, R. J. Owen, *Lett. Appl. Microbiol*. **8**, 151 (1989)]. Bacterial 16*S* ribosomal RNA primers 27F and 1522R [D. J. Lane, in *Nucleic Acid Techniques in Bacterial Systematics*, E. Stackebrandt and M. Goodfellow, Eds. (Wiley, New York, 1991), pp. 115–148] were used for the polymerase chain reaction (PCR) [R. K. Saiki *et al.*, *Science* **239**, 487 (1988)]. The amplicons were cloned into the vector PCR II (Invitrogen) and bidirectionally sequenced with dye terminator chemistry on an ABI 377 automated sequencer (Applied Biosystems, Foster City, CA). The tree in Fig. 3 was inferred from a sequence mask of 966 positions by the neighbor-joining [N. Saitou and M. Nei, *Mol. Biol. Evol*. **4**, 406 (1987)] and parsimony methods [J. Felsenstein, *PHYLIP* (University of Washington, Seattle, 1991)].
11. J. C. Priscu and H. W. Paerl, data not shown.
12. G. D. Clow, C. P. McKay, R. A. Simmons Jr., *J. Clim*. **7**, 715 (1988).
13. K. T. Wing and J. C. Priscu, *Antarct. J. U.S.* **28**, 246 (1993).
14. C. H. Fritsen and J. C. Priscu, *J. Phycol.* **34**, 493 (1998).
15. Wind-blown sediment deposits were quantified during early September before direct sunlight reached the lake. Sediments from within 100-m^2 quadrants were collected and weighed; subsamples were analyzed for POC with an elemental analyzer. These surface sediments represent aeolian deposition that had accumulated before direct sunlight and elevated temperatures induced melting when winds were highest in the area (*12*). Wind-blown sediment deposition is highest during this period (J. C. Priscu *et al.*, unpublished data) and provides an estimate of annual deposition. Replicate sediment traps (22.5-cm opening) containing 5% formalin were deployed beneath the ice for 1 year. Collected sediments were rinsed, dried, and weighed. A sediment portion was acidified with 6 M HCl, redried, and analyzed for POC.
16. C. H. Fritsen, V. I. Lytle, S. F. Ackley, C. W. Sullivan, *Science* **266**, 782 (1994).
17. M. Felip, B. Sattler, R. Psenner, J. Catalan, *Appl. Environ. Microbiol*. **61**, 2394 (1995).
18. C. P. McKay, E. I. Friedmann, R. A. Wharton, W. L. Davies, *Adv. Space Res*. **12** (no. 4), 231 (1992).
19. C. P. McKay and C. R. Stoker, *Rev. Geophys*. **27**, 189 (1989).
20. M. J. S. Belton *et al.*, *Science* **274**, 377 (1996).
21. G. W. Ojakangas and D. J. Stevenson, *Icarus* **81**, 220 (1989).
22. M. H. Carr *et al.*, *Nature* **391**, 363 (1998).
23. We thank T. Meuwissen for field assistance. Supported by the NSF (OPP 94-19423 and OPP 92-11773).

2 March 1998; accepted 20 April 1998

Gold Nanoelectrodes of Varied Size: Transition to Molecule-Like Charging

Shaowei Chen, Roychelle S. Ingram, Michael J. Hostetler, Jeremy J. Pietron, Royce W. Murray,* T. Gregory Schaaff, Joseph T. Khoury, Marcos M. Alvarez, Robert L. Whetten*

A transition from metal-like double-layer capacitive charging to redox-like charging was observed in electrochemical ensemble Coulomb staircase experiments on solutions of gold nanoparticles of varied core size. The monodisperse gold nanoparticles are stabilized by short-chain alkanethiolate monolayers and have 8 to 38 kilodaltons core mass (1.1 to 1.9 nanometers in diameter). Larger cores display Coulomb staircase responses consistent with double-layer charging of metal-electrolyte interfaces, whereas smaller core nanoparticles exhibit redox chemical character, including a large central gap. The change in behavior is consistent with new near-infrared spectroscopic data showing an emerging gap between the highest occupied and lowest unoccupied orbitals of 0.4 to 0.9 electron volt.

Nanoparticles of metals and semiconductors have sparked intense interest (*1*) in anticipation that this unexplored range of materials dimensions will yield size-dependent optical, electronic, and chemical properties suitable for applications in optoelectronic nanodevices, catalysts, and chemical sensors (*2*–*4*). Among known preparations of nanoparticles (*5*–*8*), recent attention has focused on alkanethiolate monolayer-protected metal clusters (MPCs). Gold MPCs in particular are quite stable and can be prepared with average core diameters of 1.1 to 5 nm. Electrochemical studies have demonstrated that Au MPCs are equivalent to diffusing, nanometer-sized electrodes (*9*) and can provide electrocatalytic advantages (*10*). Further, room-temperature solutions of MPCs with monodisperse cores display an electrochemical "ensemble Coulomb staircase" (*11*), a behavior anticipated and explained based on the sub-attofarad double-layer capacitances (C_{CLU}) of diffusing, nanometer-sized 28-kD metallic Au particles coated with a monolayer (hexanethiolate, C6) dielectric. Analogous staircase phenomena have been reported, using nanometer-sized electrodes (*12*).

We aim to further understand electrochemical ensemble Coulomb staircases by varying the monodisperse core mass in Au MPC solutions from 8 to 38 kD (core diameters of 1.1 to 1.9 nm). The double-layer capacitive charging seen for larger core sizes changes for smaller MPC core sizes to a molecular redox-like behavior. That is, over a certain range of core sizes, electron orbital-shell effects or pairing effects, or both, begin to dominate, changing the cluster capacitance from one determined by electrostatic processes to one more dominated by bonding interactions.

Coulomb staircases for nanoparticles are usually observed as tunneling currents through a single nanoparticle addressed by a tip probe (Fig. 1A), that undergo stepwise increments with increasing tip-substrate bias (*V*) (*13*, *14*). A model accounting for junction capacitances in a double tunnel-junction circuit (Fig. 1A) predicts that current increments occur at critical voltage biases (V_C)

$$V_C = Ze/C + (1/C)(Q_O + e/2) \quad (1)$$

where Z is integral nanoparticle charge, e the electron charge, C capacitance of the more resistive junction, and Q_O a fraction associated with tip-substrate work function differences. Coulomb staircase charging is normally observed at low temperatures because of the requirement that the stepwise charging energy ($E_C = e^2/C$) greatly exceeds thermal energy, k_BT, where k_B is Boltzmann's constant and T is temperature. Equation 1 predicts that if C is constant, consecutive charging steps should occur at a regular spacing $\Delta V_C = e/C$.

Figure 1, C and D, presents electrochemical ensemble Coulomb staircase behavior for MPCs of varied core mass, in the form of differential pulse voltammograms (DPVs) at a Pt electrode. The interfacial double-layer chargings of the uniform electronic charge and core-size MPCs with C4 and C6 coatings (*15*) produce a series of DPV current peaks (in both positive- and negative-going scans of *E*) that occur at the $\Delta V_C =$

S. Chen, R. S. Ingram, M. J. Hostetler, J. J. Pietron, R. W. Murray, Department of Chemistry, Kenan Laboratories, University of North Carolina, Chapel Hill, NC 27599–3290, USA.
T. G. Schaaff, J. T. Khoury, M. M. Alvarez, R. L. Whetten, Schools of Chemistry and Physics, Georgia Institute of Technology, Atlanta, GA 30332–0430, USA.

*To whom correspondence should be addressed. E-mail: rwm@email.unc.edu (R.W.M.) or robert.whetten@physics.gatech.edu (R.L.W.)